Paleoarchean zircons from quartzite of South Bundelkhand Supracrustal Complex: origin and implications for crustal evolution in Bundelkhand Craton, Central India

Alexander Slabunov[1], Vinod K. Singh[2], Kumar Batuk Joshi[3,4,*] and Xiaoli Li[5]

[1]Institute of Geology, Karelian Research Centre, RAS, Petrozavodsk, Russia
[2]Department of Geology, Bundelkhand University, Jhansi 284 128, India
[3]Geoscience Division, Physical Research Laboratory, Ahmedabad 380 009, India
[4]ESSO-National Centre for Earth Science Studies, Thiruvananthapuram 695 011, India
[5]School of Earth and Space Sciences, Peking University, Beijing, China

The present study reports trace elemental data from 39 Paleoarchean (3.43 and 3.25 Ga) zircons separated from quartzite near Girar, which forms a part of the South Bundelkhand Supracrustal Complex in Central India. The zircons are prismatic, have well-developed oscillatory zoning and their Th/U ratio ranging from 0.27 to 8.62 is comparable to that of typical magmatic zircons. Crystallization temperature of 620–776°C using titanium-in-zircon thermometer, positive slope of zircon REE patterns, positive Ce anomalies along with mineral inclusions like quartz, muscovite, magnetite and monazite suggest a granitic source for these quartzites. Sm–Nd isotopic data (T_{DM} age = 3.29 Ga) along with zircon trace elemental data indicate the presence of granitic continental crust in southern Bundelkhand Craton at least during the Paleoarchean (3.4 Ga).

Keywords: Bundelkhand Craton, Girar supracrustal belt, quartzites, rare earth elements, zircon chemistry.

IGNEOUS, metamorphic and sedimentary rocks contain zircons as common accessory mineral which is resistant to weathering and tends to retain age and chemical information thereby providing clues regarding the evolution of the continental crust[1]. The robust nature of zircon has been illustrated by the existence of detrital grains from Western Australia (Jack Hills)[2–6]. Numerous studies have focused on trace element chemistry[7,8] of these zircons and have been used to infer the composition, petrogenesis and provinance[2,6,9,10]. Watson and Harrison[10] proposed a granitic continental source for Hadean zircons on the basis of rare earth elements (REE) chemistry[6,11], evolved mineral inclusions like quartz[2,6], isotopic compositions[11–13] and consistently low crystallization temperatures.

This article evaluates the textural features, trace elemental compositions and crystallization temperature of 39 Paleoarchean detrital zircons from quartzite of Girar supracrustal belt from southern Bundelkhand Craton (BC) in central India. Study of these detrital zircons is crucial to understand the nature and evolution of early continental crust in BC.

Geology of Bundelkhand Craton

The Bundelkhand Crator (BC) (Figure 1 *a*) covers an area of 26,000 sq. km and consists of Archean potassium-rich granitoids[14], Archean (3.55–2.8 Ga) sodium-rich Tonalite–Trondjhemite–Granodiorites (TTGs) and Mesoarchean (ca. 2.84 Ga) to Neoarchean (2.57–2.52 Ga) greenstone complexes[15–20]. The Paleoproterozoic rocks (low metamorphosed sedimentary along with mafic flows and sills) of the Bijawar and Gwalior Groups are exposed in the southern and northern parts of BC (Figure 1 *a*). BC is delimited to the west by the Great Boundary Fault, to the northeast by the Indo-Gangetic alluvial plains and to the south, and southeast by the Vindhyan sedimentary rocks. The geology of the craton has been discussed in detail by several workers[20–26]. A dominant feature of the craton is the presence of NE–SW trending quartz veins. These quartz veins are cut by Paleoproterozoic (~2.15 Ga) mafic dykes having NNW–SSE to NW–SE trend[21,27,28].

There are two supracrustal complexes in BC[18,19]: (i) Central Bundelkhand and (ii) South Bundelkhand. The Central Bundelkhand Supracrustal Complex includes Babina and Mauranipur greenstone belts. This complex essentially consists of two associations (i) the early (Mesoarchean) sequence consisting of metamorphosed tholeiitic basalt and high Mg-basalt (basaltic association), meta-dacite–rhyolite and Banded Iron Formation (BIF), and (ii) the late (Neoarchean) felsic volcanics. On the basis of geochemical and geochronological data, subductional setting has been proposed for the formation of volcano-sedimentary rocks from Central Bundelkhand greenstone complex[18,19].

*For correspondence. (e-mail: kr.batukjoshi@gmail.com)

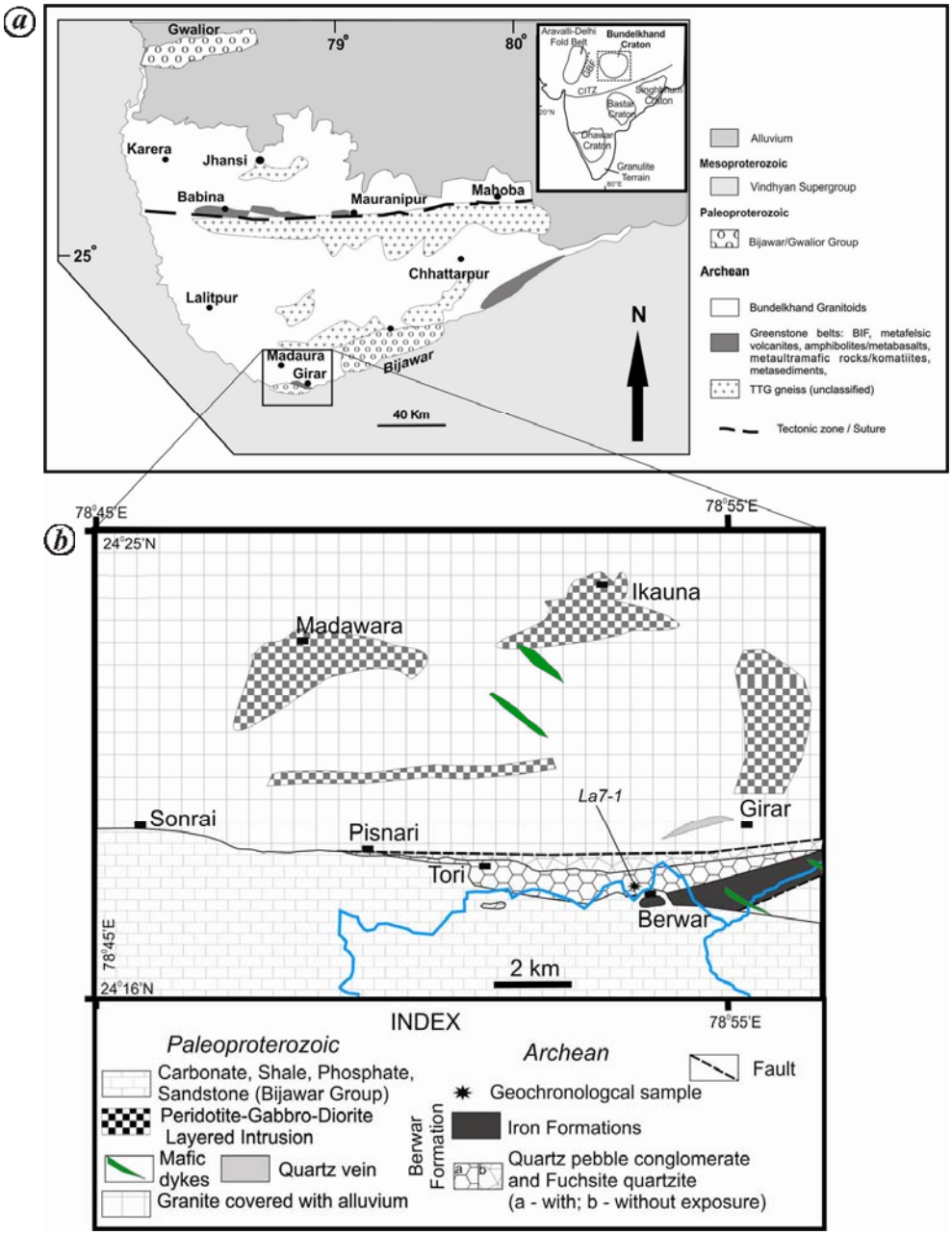

Figure 1. Geological map of the study area. ***a***, Regional geological map of Bundelkhand Craton[16,18]. (Inset) Map showing tectonic divisions of the Indian Shield[24]. ***b***, Geological map around Girar with sample location.

The South Bundelkhand Supracrustal Complex consists of Girar supracrustal belt (Figure 1 *b*). Peridotite–Gabbro–Diorite layered intrusions, viz. meta-peridotite, serpentinite, meta-gabbro and meta-pyroxenites occur in Madawara–Ikauna area[19]. The sedimentary sequence of Girar belongs to the Berwar Formation and comprises two assemblages: quartzite and BIF[19,29]. The quartzite assemblage near Berwar village is around 300 m thick and is represented by muscovite-bearing arkosic quartzite (Figure 2 *a*), fuchsite-bearing quartzite, hematite-bearing quartzite, quartz pebble conglomerates (Figure 2 *b*), dolomitic marble and traces of chlorite schist near the quartzite/BIF boundary. The BIF assemblage is around 400 m thick consisting of hematite (scarce magnetite) and quartz layers 0.5–15 mm thick (Figure 2 *c*), wherein quartz-bearing beds make up 20–95% of the rock volume.

The South Bundelkhand Supracrustal Complex lies unconformably under the gently dipping, undeformed, Paleoproterozoic rocks (conglomerates, cherts, carbonates and sandstone) of the Bijawar Group (Figure 1 *b*). This might be an indirect evidence for the older, presumably Archean age, for the rocks of Girar supracrustal belt.

Figure 2. ***a***, The occurrence of foliated muscovite–quartzite (sample La7-1) with fuchsite bearing rocks. ***b***, Quartz pebble conglomerate (left side scale in centimetre). ***c***, BIF with bands of hematite (± magnetite) and silicate phases (quartz dominant-light bands); size of coins 2.5 cm.

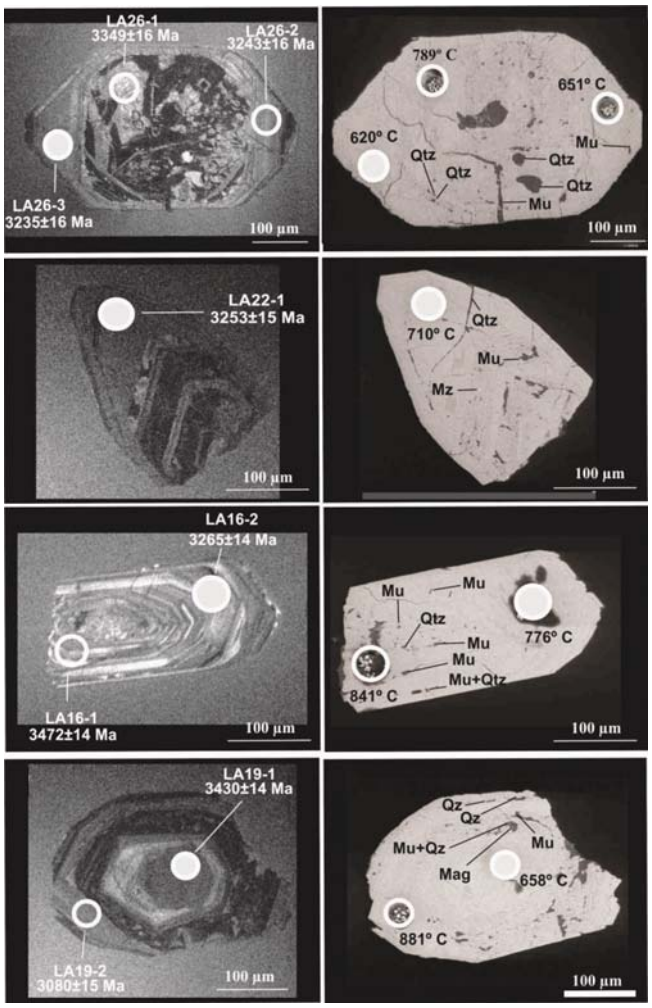

Figure 3. Cathode luminescence (CL) and backscattered electron (BSE) images of zircons from quartzite of Girar supracrustal belt showing the respective inclusions and titanium-in-zircon temperatures. Filled and blank circles mark the areas from which concordant and discordant ages were obtained.

Trace element analysis of zircon

Zircons were separated from 2 kg of quartzite sample (La7-1) (Figure 2 *a*) collected from the Girar supracrustal belt. The sample was crushed and heavy minerals were concentrated by gravitational, magnetic and electrical methods. Heavy mineral separation was done with heavy liquids and finally the heavy fractions were hand-picked for zircons under a binocular microscope. Further, the zircons were mounted in epoxy resin and well-polished to expose their cores. The zircons were investigated under optical microscope and Cathode luminescence (CL) images were obtained to characterize the internal structure (Figure 3) of zircons using a scanning electron microscope (QUANTA-650FEG, equipped with INCA-Synergy and CHROMA-D detectors) at Peking University, China. *In situ* analysis of trace elements was performed using mass spectrometry (ICP-MS Agilent 7500 Ce equipped with a Complex Pro102 laser ablation system (LA-ICP-MS)) at Peking University, China, with a precision of ±7%. Mineral chemistry of inclusions in zircon and backscattered electron (BSE) images was studied using 15 kV accelerating voltage, 15 ± 0.05 nA beam current and 10–15 s counting time utilizing an electron microscope (Vega II LSH) in the Institute of Geology at the Karelian Research Centre, Russia.

Zircons separated from the studied quartzite samples are large (300–500 µm), transparent and pink in colour, and lack effects of abrasion. They are doubly terminated prismatic crystals with {101} dominant forms and elongation ratios of 1.5–3. Thin oscillatory zoning and xenocrystic cores (Figure 3) are visible in the CL images (which is common for magmatic zircons)[30,31]. In addition, the studied zircons have typical magmatic Th/U ratio of 0.27–8.62. The cores are usually distinct on the CL images and some of them show traces of recrystallization like presence of convolute zoning (Figure 3). Mineral inclusions in the cores and rims of zircons contain evidence of old granitic protolith with inclusions like quartz, muscovite, magnetite and monazite which are characteristic of granitoids (Figure 3).

The REE contents in zircon are in general related to the systematic variation of REE^{3+} ionic radii which in turn gives them a positive slope in chondrite normalized REE diagrams[32–37]. Comparison of the various REE patterns

Table 1. Trace element concentration in zircons from quartzite (sample La7-1) of Girar supracrustal belt

Spot no.	LA-1-1 Rim Discordant	LA-1-2 Core Discordant	LA-2-1 Core Discordant	LA-3-1 Core Discordant	LA-4-1 Core Discordant	LA-5-1 Core Discordant	LA-6-1 Core Discordant	LA-6-2 Rim Concordant
Age[a]	3135	2807	2930	2588	2741	3318	3237	3249
1σ	12.00	12.00	12.00	13.00	13.00	42.00	12.00	13.00
Ti	491.07	591.87	65.93	699.09	435.32	30.25	57.41	3.10
Y	3322.99	3518.73	1924.18	6361.63	6257.51	1465.45	1396.68	240.28
La	114.86	94.69	19.28	147.98	75.10	6.84	15.01	1.12
Ce	1280.12	1131.33	217.61	1274.89	776.63	93.96	165.56	13.78
Pr	220.58	191.24	36.51	201.72	124.28	10.57	25.88	1.89
Nd	1455.41	1293.48	226.43	1193.85	719.92	64.63	146.60	10.18
Sm	570.28	548.81	134.12	675.83	387.91	38.88	71.23	5.05
Eu	256.38	239.07	90.61	443.08	268.05	24.11	48.50	3.36
Gd	801.28	798.00	244.91	1111.25	697.98	91.06	138.41	10.33
Tb	81.57	80.18	39.14	183.27	137.04	19.08	26.16	2.50
Dy	412.11	402.20	233.46	972.86	872.82	151.60	177.16	21.89
Ho	90.94	95.74	57.23	187.42	195.94	45.13	44.54	7.54
Er	309.79	361.66	211.07	545.58	595.24	183.72	157.52	33.90
Tm	66.72	84.90	46.73	109.11	103.38	39.70	31.15	8.32
Yb	695.78	871.56	475.11	1183.89	892.68	394.72	298.00	94.48
Lu	125.49	155.11	84.96	230.20	146.76	69.98	54.34	18.18
Th	1615.62	1405.28	1284.23	12288.22	3316.41	242.73	1369.20	75.12
U	1138.34	1382.01	718.26	1425.68	1624.90	225.43	250.03	81.81
T[b]	1258	1296	939	1332	1234	848	922	647[c]

Spot no.	LA-7-1 Core Discordant	LA-7-2 Rim Discordant	LA-8-1 Rim Discordant	LA-9-1 Core Concordant	LA-10-1 Core Discordant	LA-11-1 Core Discordant	LA-11-2 Rim Discordant	LA-12-1 Core Discordant
Age[a]	2883	3225	2699	3434	3237	3146	3259	3088
1σ	13.00	13.00	13.00	13.00	13.00	14.00	13.00	14.00
Ti	118.00	68.63	173.20	9.21	20.53	20.65	96.99	31.76
Y	1014.12	932.60	2838.34	655.28	586.57	840.66	1919.12	830.75
La	30.20	20.38	38.60	3.87	5.69	7.46	30.12	8.95
Ce	268.80	209.58	421.68	29.35	67.98	98.25	296.90	77.65
Pr	48.69	35.13	68.87	2.86	11.42	10.28	48.81	10.85
Nd	316.91	216.16	406.50	16.21	71.32	58.72	266.68	60.09
Sm	115.67	80.87	214.98	7.63	28.54	48.07	131.82	28.24
Eu	46.00	35.00	143.92	2.08	12.82	36.85	84.73	19.42
Gd	151.74	127.44	363.68	20.93	49.24		233.20	56.63
Tb	14.65	15.12	63.68	6.20	6.82	7.07	42.03	12.18
Dy	93.78	98.28	381.20	65.86	53.83	111.05	265.23	93.87
Ho	30.28	27.89	83.12	23.05	18.56	29.55	58.16	25.23
Er	140.24	112.31	266.70	96.94	80.63	121.55	180.44	100.63
Tm	35.63	25.23	53.97	20.05	18.00	27.17	35.21	21.35
Yb	384.89	257.61	555.39	185.68	186.77	286.14	345.09	224.01
Lu	75.43	47.78	101.11	31.55	35.93	42.55	61.97	42.56
Th	356.08	421.43	714.53	182.97	111.73	2096.26	753.26	1429.14
U	875.48	348.87	1101.43	122.72	169.35	416.99	471.18	417.53
T[b]	1017	944	1074	734	808	990	854	927

Spot no.	LA-13-1 Core Discordant	LA-14-1 Core Discordant	LA-14-2 Rim Discordant	LA-15-1 Rim Discordant	LA-16-1 Core Concordant	LA-16-2 Rim Discordant	LA-17-1 Core Discordant	LA-17-2 Rim Discordant
Age[a]	3433	3218	3239	3472	3265	1625	3188	3063
1σ	13.00	14.00	14.00	14.00	14.00	147.00	14.00	15.00
Ti	60.04	16.62	18.64	52.74	28.30	14.76	1024.61	145.49
Y	1259.16	606.01	737.91	728.14	1209.06	958.27	5621.42	1652.92
La	18.33	6.44	7.26	13.75	10.13	3.58	218.09	46.17
Ce	184.16	54.11	65.64	135.16	109.09	39.33	2315.12	454.89
Pr	28.95	8.16	10.07	23.50	18.08	5.64	398.90	77.93
Nd	155.34	38.91	51.43	133.54	105.42	29.67	2649.25	471.60
Sm	73.02	18.33	21.91	60.15	48.12	14.43	1103.19	185.27

(*Contd*)

Table 1. (*Contd*)

Spot no.	LA-13-1 Core Discordant	LA-14-1 Core Discordant	LA-14-2 Rim Discordant	LA-15-1 Rim Discordant	LA-16-1 Core Concordant	LA-16-2 Rim Discordant	LA-17-1 Core Discordant	LA-17-2 Rim Discordant
Eu	49.71	10.36	14.40	35.80	30.03	8.51	480.96	83.16
Gd	131.46	37.46	44.89	109.76	96.37	34.21	1496.07	284.27
Tb	24.30	8.14	9.83	17.04	18.73	8.93	141.99	31.09
Dy	160.39	64.76	76.08	99.06	139.20	88.52	683.15	179.50
Ho	37.68	19.47	24.05	21.18	38.62	32.17	150.29	46.42
Er	124.47	76.33	100.37	63.84	144.52	143.06	533.02	178.06
Tm	24.54	16.35	22.85	11.66	28.36	32.53	118.33	40.62
Yb	231.38	160.31	230.77	105.91	265.11	327.70	1297.93	422.48
Lu	41.39	29.01	44.49	17.42	46.20	58.11	235.67	77.10
Th	760.83	738.40	1462.49	621.67	228.38	2734.00	1225.70	4288.00
U	137.57	252.22	431.00	121.48	278.58	1939.96	509.47	845.93
T^b	788	799	912	841	776	1421	1047	1118
Spot no.	LA-18-1 Core Discordant	LA-18-2 Rim Concordant	LA-19-1 Core Discordant	LA-19-2 Rim Concordant	LA-20-1 Core Discordant	LA-20-2 Rim Concordant	LA-21-1 Core Concordant	LA-21-2 Rim Discordant
Age[a]	3189	3430	3080	3247	3203	3265	3253	2982
1σ	15.00	14.00	15.00	15.00	15.00	15.00	15.00	16.00
Ti	227.99	118.42	5.09	40.69	9.99	19.25	9.25	169.72
Y	2134.79	1977.82	633.43	1154.27	786.21	828.63	206.16	3175.44
La	45.36	32.12	0.69	8.25	0.93	5.56	1.43	40.10
Ce	388.03	274.78	14.62	97.76	16.17	63.82	18.74	413.01
Pr	64.14	45.46	1.11	14.42	1.61	9.56	2.33	67.03
Nd	348.40	245.64	6.32	81.67	9.10	53.55	14.08	376.92
Sm	171.87	110.53	4.84	45.84	6.51	26.27	7.22	187.37
Eu	114.62	71.76	2.15	29.71	3.92	17.58	5.02	125.10
Gd	271.97	203.17	16.24	83.02	22.11	53.92	11.56	339.37
Tb	47.44	39.65	5.17	18.23	6.58	11.85	2.78	64.82
Dy	279.05	256.83	57.87	132.64	70.17	93.20	21.59	427.03
Ho	62.79	59.73	21.83	36.87	26.00	26.07	6.36	95.87
Er	229.16	193.71	95.97	143.71	115.67	102.83	26.56	307.05
Tm	52.03	38.31	21.37	30.33	25.70	22.68	5.94	60.37
Yb	572.16	374.02	211.70	304.04	259.21	231.65	64.97	593.28
Lu	111.26	66.50	38.51	57.33	47.64	41.74	11.96	104.92
Th	1979.94	113.34	261.94	113.74	177.70	64.68	64.00	1139.76
U	503.30	200.15	447.53	250.09	298.21	194.46	237.62	903.84
T^b	1017	685	881[c]	741	802	734	710	1071
Spot no.	LA-22-1 Rim Discordant	LA-23-1 Rim Discordant	LA-24-1 Rim Discordant	LA-25-1 Rim Discordant	LA-26-1 Core Discordant	LA-26-2 Rim Concordant	LA-26-3 Rim Discordant	LA-27-1 Rim Discordant
Age[a]	3214	3162	3148	3349	3243	3235	3349	1625
1σ	16.00	16.00	16.00	16.00	16.00	16.00	16.00	147.00
Ti	7.00	34.13	123.83	52.75	16.91	3.26	<2.09	31.27
Y	980.51	754.20	2543.74	1950.83	372.20	272.93	346.25	718.81
La	3.54	13.62	42.37	6.61	1.58	<0.030	<0.028	11.48
Ce	48.89	122.23	446.38	97.30	18.82	5.81	7.67	110.61
Pr	6.28	19.29	70.39	14.25	3.04	<0.026	<0.023	19.42
Nd	36.93	115.25	381.60	84.51	18.47	0.14	0.19	103.16
Sm	18.36	43.78	163.35	45.37	12.02	0.52	0.79	42.71
Eu	12.18	21.69	114.82	27.52	8.22	0.21	0.24	28.19
Gd	42.71	74.82	292.42	102.20	22.64	4.16	5.80	77.94
Tb	10.17	10.71	58.91	24.67	4.43	1.72	2.33	15.02
Dy	92.56	76.22	380.98	206.24	33.10	22.91	30.19	93.60
Ho	32.16	22.03	79.97	61.28	10.53	9.12	12.12	21.46
Er	139.81	87.71	239.27	237.94	50.53	45.04	56.15	70.68
Tm	30.06	19.34	43.35	51.02	14.38	10.88	13.38	15.31
Yb	300.76	200.05	387.64	502.01	180.47	114.73	142.59	159.34
Lu	52.16	35.43	64.36	84.76	37.60	20.40	24.78	30.17
Th	152.70	1502.76	157.81	120.02	48.86	60.03	903.72	2734.00
U	267.89	553.39	364.75	447.26	165.54	182.53	208.46	1939.96
T^b	862	1024	912	789	651	620[c]	852[c]	1420

[a]$^{207}Pb/^{206}Pb$ age in Ma and 1σ for this age; T^b Temperature in °C (1σ is 15°–26°C); where at [c]1σ is 36–60°C.

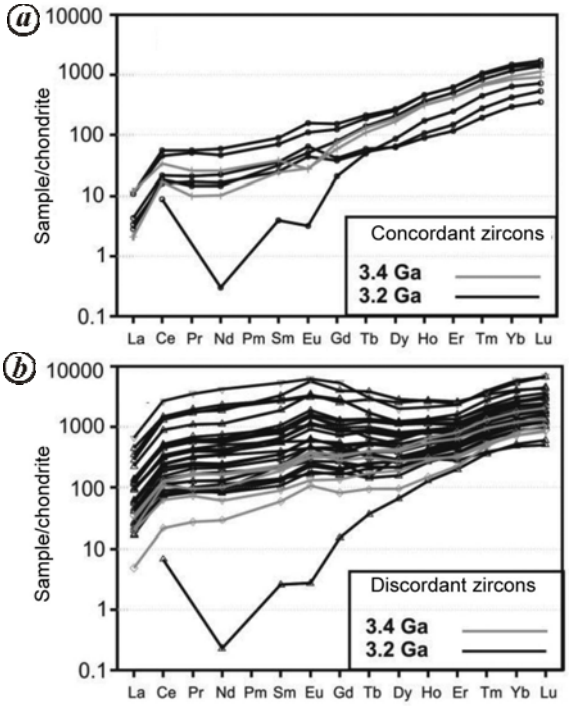

Figure 4. Chondrite-normalized REE patterns for (***a***) concordant; and (***b***) discordant zircons from quartzite of Girar supracrustal belt.

demonstrates that the rims of the zircon grains have similar concentrations of REEs. On the basis of REE chemistry, the analysed zircons can be separated into two subgroups depending on concordant or discordant relations (Table 1). Most of the zircons (except one) which give concordant ages have lower LREE enrichment compared to those with discordant relations which exhibit much more enriched LREE (Figure 4). Both zircon groups show positive slope with similarly enriched HREE content (Figure 4). Most of the concordant zircons show slightly positive Eu anomalies, except for two older grains which show slight depletion in Eu concentration. On the other hand, most of the discordant zircons have elevated LREE content and slightly positive or no Eu anomaly (Figure 4). Presence of Ce anomaly in the REE patterns may be due to presence of Ce^{4+}, which is more compatible in zircon than trivalent Ce^{3+}. The magnitude of this anomaly depends on the redox condition of the melt/fluid from which the zircon has crystallized[38].

Results and discussion

The application of zircon geochemistry to study geologic processes extends beyond geochronology. Partial or total loss of Pb is a common feature during magmatic and metamorphic zircon growth due to alteration caused by later fluids[39–45]. Large variations in Ti and other trace-element concentrations as in the case of the studied detrital zircons might be due to repeated influxes of hotter fluids which might be caused by changes in the temperature or composition of melts parental to zircons[35,46–49]. The Eu anomaly suggests plagioclase fractionation in the magma and is in line with a magmatic origin of the zircons. All the studied zircon populations also have a positive Ce anomaly (Figure 4); which might have originated from the oxidation of Ce^{3+} to Ce^{4+}, that better fits the Zr site in zircon[33].

The REE patterns from zircons show that their discordance correlates with the chondrite-normalized rare earth patterns. The chondrite normalized La contents <25 ppm and Yb_N values less than 10,000, positive Ce and Th/U > 0.3 suggest that the studied concordant zircons are of igneous origin[31,50]. This is also corroborated by the slope of the REE patterns which is fairly uniform, showing Gd_N/La_N and Yb_N/Gd_N ratios of <30. On the contrary, features like elevated Y, La_N, and LREE concentration in zircons with higher discordance (Figure 4, Table 1), might be due to later hydrothermal processes[30,50,51]. The above-mentioned geochemical features suggest that the zircons from quartzite of Girar supracrustal belt are a mix of magmatic and hydrothermally altered zircons. It is to be noted that zircons from the studied quartzites lack abrasions thus pointing towards proximity to source.

Watson and Harrison[10] and Watson *et al.*[51] experimentally calibrated the titanium concentration in zircon as a function of temperature of formation and the activity of TiO_2. Titanium-in-zircon thermometry has been applied to a growing number of natural zircons[10,52,53]. Titanium-in-zircon temperatures ranging from 620°C to 776°C were estimated from quartzite of Girar supracrustal belt (Table 1). It is to be noted that a majority of the discordant zircons show much higher titanium-in-zircon temperatures compared to concordant ones (Table 1), which might be due to inputs from later hydrothermal fluids. The calculated crystallization temperatures from quartzite are similar to average crystallization temperatures of Early Archean detrital zircons, thereby pointing towards granitic parent magma[10,52,54]. This is also corroborated by the presence of zircon inclusions like quartz, muscovite, magnetite and monazite which are characteristic of granitoids (Figure 3).

U–Pb zircon data from quartzite of Girar supracrustal belt, give an older age of 3.43 Ga and younger age of 3.25 Ga (ref. 55), suggesting 3.25 Ga to be the minimum age of the source sediments. Whole-rock Sm–Nd analysis of quartzite gives a depleted mantle Nd (T_{DM}) model age of 3.29 Ga which is similar to the U–Pb age of the analysed zircons[55], thereby indicating that the continental crust of the southern part of BC formed during the Paleoarchean (3.4–3.3 Ga). It can be summarized that the quartzites of Girar supracrustal belt were produced by the reworking of granitoids, whose zircons clearly dominate in sediments. The presence of Paleoarchaean continental (granitoid) crust in the source area cannot be ignored, which is clearly evident by the presence of

zircons as old as 3.4 Ga in the studied quartzites and available U–Pb zircon data of previously studied TTGs from BC[16–19]. The nature and age obtained from quartzite of Girar supracrustal complex suggest that the continental crust in southern Bundelkhand formed during two Paleoarchean events (3.43 Ga and 3.35 Ga) due to reworking of the pre-existing continental crust.

1. Grimes, C. B. *et al.*, The trace element chemistry of zircons from oceanic crust: a method for distinguishing detrital zircon provenance. *Geology*, 2007, **35**, 643–646.
2. Wilde, S. A., Valley, J. W., Peck, W. H. and Graham, C. M., Evidence from detrital zircons for the existence of continental crust and oceans on the earth 4.4 Gyr ago. *Nature*, 2001, **409**, 175–178.
3. Cavosie, A. J., Valley, J. W. and Wilde, S., The oldest terrestrial mineral record: a review of 4400 to 4000 Ma detrital zircons from Jack Hills, Western Australia. *Dev. Precambrian Geol.*, 2007, **15**, 91–111.
4. Harrison, T. M., The Hadean crust: evidence from >4 Ga zircons. *Annu. Rev. Earth Planet. Sci.*, 2009, **37**, 479–505.
5. Bowring, S. A. and Williams, I. S., Priscoan (4.00–4.03 Ga) orthogneisses from northwestern Canada. *Contrib. Mineral. Petrol.*, 1999, **134**, 3–16.
6. Maas, R., Kinny, P. D., Williams, I. S., Froude, D. O. and Compston, W., The earth's oldest known crust: a geochronological and geochemical study of 3900–4200 Ma detrital zircons from Mt Narryer and Jack Hills, Western Australia. *Geochim. Cosmochim. Acta*, 1992, **56**, 1281–1300.
7. Hoskin, P. W. O. and Ireland, T. R., Rare earth element chemistry of zircon and its use as a provenance indicator. *Geology*, 2000, **28**, 627–630.
8. Belousova, E. A., Griffin, W. L., O'Reilly, S. and Fisher, N. I., Igneous zircon: trace element composition as an indicator of source rock type. *Contrib. Mineral. Petrol*, 2002, **143**, 602–622.
9. Valley, J. W., Peck, W. H., King, E. M. and Wilde, S. A., A cool early earth. *Geology*, 2002, **30**, 351–354.
10. Watson, E. B. and Harrison, T. M., Zircon thermometer reveals minimum melting conditions on earliest earth. *Science*, 2005, **308**, 841–844.
11. Peck, W. H., Valley, J. W., Wilde, S. A. and Graham, C. M., Oxygen isotope ratios and rare earth elements in 3.3 to 4.4 Ga zircons: ion microprobe evidence for high d18O continental crust and oceans in the Early Archean. *Geochim. Cosmochim. Acta*, 2001, **65**, 4215–4229.
12. Valley, J. W. *et al.*, 4.4 billion years of crustal maturation: oxygen isotopes in magmatic zircon. *Contrib. Mineral. Petrol.*, 2005, **150**, 561–580.
13. Harrison, T. M., Blichert-Toft, J., Muller, W., Albarede, F., Holden, P. and Mojzsis, S. J., Heterogeneous Hadean hafnium: evidence of continental crust at 4.4 to 4.5 Ga. *Science*, 2005, **310**, 1947–1950.
14. Verma, S. K. Verma, S. P., Oliveira, E. P., Singh, V. K. and More, J. A. LA-SF-ICP-MS zircon U–Pb geochronology of granitic rocks from the central Bundelkhand greenstone complex, Bundelkhand craton, India. *J. Asian Earth Sci.*, 2016, **118**, 125–137.
15. Sarkar, A., Paul, D. K. and Potts, P. J., Geochronology and geochemistry of the Mid-Archaean, Trondhjemitic gneisses from the Bundelkhand craton, Central India. In *Recent Researches in Geology* (ed. Saha, A. K.), 1996, vol. 16, pp. 76–92.
16. Mondal, M. E. A., Goswami, J. N., Deomurari, M. P. and Sharma, K. K., Ion microprobe $^{207}Pb/^{206}Pb$ ages of zircon from the Bundelkhand massif, northern India: implication for crustal evolution of Bundelkhand – Aravalli protocontinent. *Precamb. Res.*, 2002, **117**, 85–100.
17. Kaur, P., Zeh, A. and Chaudhri, N., Characterisation and U–Pb–Hf isotope record of the 3.55 Ga felsic crust from the Bundelkhand Craton, northern India. *Precamb. Res.*, 2014, **255**, 236–244.
18. Singh, V. K. and Slabunov, A., The Central Bundelkhand Archaean greenstone complex, Bundelkhand craton, central India: geology, composition, and geochronology of supracrustal rocks. *Int. Geol. Rev.*, 2015, **57**(11–12), 1349–1364.
19. Singh, V. K. and Slabunov, A., Two types of Archaean supracrustal belts in the Bundelkhand Craton, India: geology, geochemistry, age and implication for craton crustal evolution. *J. Geol. Soc. India*, 2016, **88**, 539–548.
20. Joshi, K. B. *et al.*, The diversification of granitoids and plate tectonic implications at the Archaean–Proterozoic boundary in the Bundelkhand Craton, Central India. In *Crust–Mantle Interactions and Granitoid Diversification: Insights from Archaean Cratons* (eds Halla, J. *et al.*), Special Publications, Geological Society, London, 2016, vol. 449; http://doi.org/10.1144/SP449.8.
21. Basu, A. K., Geology of parts of Bundelkhand granite massif, Central India. *Rec. Geol. Surv. India*, 1986, **117**, 61–124.
22. Mondal, M. E. A. and Zainuddin, S. M., Geochemical characteristics of the granites of Bundelkhand massif, Central India. *J. Geol. Soc. India*, 1997, **50**, 69–74.
23. Malviya, V. P., Arima, M., Pati, J. K. and Kaneko, Y., Petrology and geochemistry of metamorphosed basaltic pillow lava and basaltic komatiite in the Mauranipur area: subduction related volcanism in the Archaean Bundelkhand craton, Central India. *J. Mineral. Petrol. Sci.*, 2006 **101**, 199–217.
24. Ramakrishnan, M. and Vaidyanadhan, R., *Geology of India*, Geological Society of India, Bangalore, 2010, p. 556.
25. Mohan, M. R., Singh, S. P., Santosh, M., Siddiqui, M. A. and Balaram, V., TTG suite from the Bundelkhand craton, Central India: geochemistry, petrogenesis and implications for Archaean crustal evolution. *J. Asian Earth Sci.*, 2012, **58**, 38–50.
26. Singh, V. K. and Slabunov, A., Geochemical characteristics of banded iron formation and metavolcanics of Babina greenstone belt of the Bundelkhand Craton, Central India. *J. Econ. Geol. Georesour. Manage.*, 2015, **10**, 63–74.
27. Rao, J. M., Rao, G. V. S. P., Widdowson, M. and Kelley, S. P., Evolution of Proterozoic mafic dyke swarms of the Bundelkhand Granite Massif, Central India. *Curr. Sci.*, 2005, **88**, 502–506.
28. Pradhan, V. R. *et al.*, Paleomagnetic and geochronological studies of the mafic dyke swarms of Bundelkhand craton, central India: implications for the tectonic evolution and paleogeographic reconstructions. *Precamb. Res.*, 2012, **198–199**, 51–76.
29. Pascoe, E. H., *A Manual of the Geology of India and Burma*, Government of India Press, Calcutta, 1950, vol. I, pp. 246–293.
30. Fujimaki, H., Partition coefficients of Hf, Zr, and REE between zircon, apatite, and liquid. *Contrib. Mineral. Petrol.*, 1986, **94**, 42–45.
31. Hoskin, P. W. O. and Schaltegger, U., The composition of zircon and igneous and metamorphic petrogenesis. *Rev. Mineral. Geochem.*, 2002, **53**, 27–62.
32. Hanchar, J. M. *et al.*, Rare earth elements in synthetic zircon: Part 1. Synthesis, and rare earth element and phosphorus doping. *Am. Miner.*, 2001, **86**, 667–680.
33. Heaman, L. M., Bowins, R. and Crocket, J., The chemical composition of igneous zircon suites: implications for geochemical tracer studies. *Geochim. Cosmochim. Acta*, 1990, **54**, 1597–1607.
34. Hinton, R. W. and Upton, B. G. J., The chemistry of zircon: variations within and between large crystals from syenite and alkali basalt xenoliths. *Geochim. Cosmochim. Acta*, 1991, **55**, 3287–3302.
35. Nagasawa, H., Rare earth concentrations in zircons and apatites and their host dacites and granites. *Earth Planet. Sci. Lett.*, 1970, **9**, 359–364.
36. Watson, E. B., Some experimentally determined zircon/liquid partition coefficients for the rare earth elements. *Geochim. Cosmochim. Acta*, 1980, **44**, 895–897.

37. Ballard, J. R., Palin, M. J. and Campbell, I. H., Relative oxidation states of magmas inferred from Ce(IV)/Ce(III) in zircon: application to porphyry copper deposits of northern Chile. *Contrib. Miner. Petrol*, 2002, **144**, 347–364.
38. Nasdala, L. *et al.*, Metamictisation of natural zircon: accumulation versus thermal annealing of radioactivity-induced damage. *Contrib. Mineral. Petrol.*, 2001, **141**, 125–144.
39. Rubatto, D., Zircon trace element geochemistry: distribution coefficients and the link between U–Pb ages and metamorphism. *Chem. Geol.*, 2002, **184**, 123–138.
40. Rubatto, D. and Hermann, J., Zircon formation during fluid circulation in eclogites (Monviso, Western Alps): implications for Zr and Hf budget in subduction zones. *Geochim. Cosmochim. Acta*, 2003, **67**, 2173–2187.
41. Zheng, Y. F., Wu, Y. B. and Zhao, Z. F., Metamorphic effect on zircon Lu–Hf and U–Pb isotope systems in ultrahigh-pressure metagranite and metabasite. *Earth Planet. Sci. Lett.*, 2005, **240**, 378–400.
42. Zheng, Y. F., Gao, T. S., Wu, Y. B. and Gong, B., Fluid flow during exhumation of deeply subducted continental crust: zircon U–Pb age and O isotope studies of quartz vein in eclogite. *J. Metamorph. Geol.*, 2007, **25**, 267–283.
43. Schaltegger, U., Hydrothermal zircon. *Elements*, 2007, **3**, 51–79.
44. Chen, R. X., Zheng, Y. F. and Xie, L. W., Metamorphic growth and recrystallization of zircon: distinction by simultaneous *in situ* analyses of trace elements, U–Th–Pb and Lu–Hf isotopes in zircons from eclogite-facies rocks in the Sulu orogeny. *Lithos*, 2010, **114**, 132–154.
45. Bolhar, R. *et al.*, Sources and evolution of arc magmas inferred from coupled O and Hf isotope systematics of plutonic zircons from the cretaceous separation point suite (New Zealand). *Earth Planet. Sci. Lett.*, 2008, **268**(3–4), 312–324.
46. Carley, T. L., Miller, C. F., Wooden, J. L., Bindeman, I. N. and Barth, A. P., Zircon from historic eruptions in Iceland: reconstructing storage and evolution of silicic magmas. *Mineral. Petrol.*, 2011, **102**, 135–161.
47. Claiborne, L. L., Miller, C. F., Flanagan, D. M., Clynne, M. A. and Wooden, J. L., Zircon reveals protracted magma storage and recycling beneath Mount St Helens. *Geology*, 2010, **38**, 1011–1014.
48. Stelten, M. and Cooper, K. M., Constraints on the nature of the subvolcanic system at South Sister Volcano, Oregon from ^{238}U–^{230}Th zircon ages and ^{238}U–^{230}Th–^{226}Ra plagioclase ages. Abstracts with Programs. Geological Society of America, 2010, vol. 42, p. 668.
49. Walker, B., Grunder, A. and Wooden, J., Organization and thermal maturation of long-lived arc systems: evidence from zircons at the Aucanquilcha volcanic cluster, northern Chile. *Geology*, 2010, **38**, 1007–1010.
50. Toscano, M., Pascual, E. and Nesbitt, R. W., Geochemical discrimination of hydrothermal and igneous zircon in the Iberian Pyrite Belt Spain. *Ore Geol. Rev.*, 2014, **56**, 301–311.
51. Watson, E. B., Wark, D. A. and Thomas, J. B., Crystallization thermometers for zircon and rutile. *Contrib. Miner. Petrol.*, 2006, **151**, 413–433.
52. Fu, B. *et al.*, Ti-in-zircon thermometry: applications and limitations. *Contrib. Mineral. Petrol.*, 2008, **156**, 197–215.
53. Watson, E. B. and Harrison, T. M., Response to comments on 'Zircon thermometer reveals minimum melting conditions on earliest earth'. *Science*, 2006, **311**, 779.
54. Harrison, T. M., Watson, E. B. and Aikman, A. B., Temperature spectra of zircon crystallization in plutonic rocks. *Geology*, 2007, **35**, 635–638.
55. Slabunov, A., Nazarova, D., Li, X. and Singh, V. K., The role of the paleoarchaean continental crust in the Bundelkhand Craton, Central India: the results of Sm–Nd and U–Pb isotopic studies. In International Association for Gondwana Research Conference Series No. 16, 3rd International Conference on Precambrian Continental Growth and Tectonism (eds Singh, V. K. and Chandra, R.), Jhansi, 2013, pp. 178–179.

ACKNOWLEDGEMENT. This article is a contribution to RFBR grants 13-05-91162, 15-35-50162 and 17-55-45005. We thank Institute of Geology Karelian RC RAS, School of Earth and Space Sciences, Peking University and the Director of the ESSO-National Centre for Earth Science Studies for support.

Received 10 July 2015; revised accepted 16 September 2016

doi: 10.18520/cs/v112/i04/794-801